The impact of rising CO_2 and acclimation on the response of US forests to global warming

John S. Sperry[a,1], Martin D. Venturas[a,1,2], Henry N. Todd[a], Anna T. Trugman[a,b], William R. L. Anderegg[a], Yujie Wang[a], and Xiaonan Tai[c]

[a]School of Biological Sciences, University of Utah, Salt Lake City, UT 84112; [b]Department of Geography, University of California, Santa Barbara, CA 93106; and [c]Department of Geology and Geophysics, University of Utah, Salt Lake City, UT 84112

The response of forests to climate change depends in part on whether the photosynthetic benefit from increased atmospheric CO_2 (ΔC_a = future minus historic CO_2) compensates for increased physiological stresses from higher temperature (ΔT). We predicted the outcome of these competing responses by using optimization theory and a mechanistic model of tree water transport and photosynthesis. We simulated current and future productivity, stress, and mortality in mature monospecific stands with soil, species, and climate sampled from 20 continental US locations. We modeled stands with and without acclimation to ΔC_a and ΔT, where acclimated forests adjusted leaf area, photosynthetic capacity, and stand density to maximize productivity while avoiding stress. Without acclimation, the ΔC_a-driven boost in net primary productivity (NPP) was compromised by ΔT-driven stress and mortality associated with vascular failure. With acclimation, the ΔC_a-driven boost in NPP and stand biomass (C storage) was accentuated for cooler futures but negated for warmer futures by a ΔT-driven reduction in NPP and biomass. Thus, hotter futures reduced forest biomass through either mortality or acclimation. Forest outcomes depended on whether projected climatic $\Delta C_a/\Delta T$ ratios were above or below physiological thresholds that neutralized the negative impacts of warming. Critically, if forests do not acclimate, the $\Delta C_a/\Delta T$ must be above ca. 89 ppm·°C^{-1} to avoid chronic stress, a threshold met by 55% of climate projections. If forests do acclimate, the $\Delta C_a/\Delta T$ must rise above ca. 67 ppm·°C^{-1} for NPP and biomass to increase, a lower threshold met by 71% of projections.

acclimation | climate change | drought | forest resilience | vegetation modeling

The future will continue to bring elevated atmospheric CO_2 (C_a) and warmer temperatures (T) to the world's forests (1). These 2 atmospheric shifts (ΔC_a = elevated CO_2, ΔT = climatic warming) can have opposite effects on the uptake and storage of CO_2 by trees and influence their potential to mitigate further increases in C_a. A ΔC_a in isolation typically stimulates photosynthesis (2) and can "fertilize" an increase in forest net primary productivity (NPP) (photosynthesis minus autotrophic respiration) as free air CO_2 enrichment (FACE) studies have shown (3, 4). If CO_2 fertilization is accompanied by greater tree and ecosystem carbon storage, trees will continue to slow the rise in C_a from fossil fuel emissions (4, 5). However, climate change also brings ΔT, which can have the opposite effect from ΔC_a. Warmer air will have a greater vapor pressure deficit (D) (6), which can reduce photosynthesis by inducing stomatal closure, both directly in response to greater transpiration (7) and indirectly in response to faster soil drying by root uptake (8). In extremis, ΔT contributes to drought-related mortality (9, 10). The negative influences of ΔT would contribute to a faster rise in C_a. There is already evidence for both positive and negative impacts of climate change on forests globally (5, 11–13), and the response is complicated beyond basic physiology by changing land use, fire regimes, pathogen and pest impact, species turnover, and other factors. Here we focus on the fundamental question of how trees will respond physiologically to

the conflicting stimuli of ΔC_a and ΔT and the implications for future forests.

While the competing influences of ΔC_a and ΔT on tree function are well-established empirically, experiments with trees have inherent difficulties distinguishing shorter-term physiological responses from longer-term adjustments (here termed "acclimation") to a new steady state. Short-term stimulation of growth by ΔC_a does not necessarily mean an increase in the biomass carrying capacity of a mature forest (14). Acclimation, particularly in notably plastic traits of individual tree leaf area (LA) and leaf photosynthetic capacity (carboxylation capacity, V_{max25}; and electron transport capacity, J_{max25} at 25 °C), can alter the leaf-level response to ΔC_a and ΔT over time (2, 15–18). Stand structure, especially the density of trees (basal area per ground area, BAI), forest LA per ground area (LAI), and tree rooting depth, combine to determine the level of resource competition, which also influences a tree's response to a given ΔC_a or ΔT. Given the roles of growth, stress-avoiding acclimation, and resource availability, it is not surprising that widespread variability in forest responses is often observed across ΔC_a and ΔT experiments (3, 4, 19).

Significance

The benefit of climate change for forests is that higher atmospheric CO_2 allows trees to use less water and photosynthesize more. The problem of climate change is that warmer temperatures make trees use more water and photosynthesize less. We predicted the outcome of these opposing influences using a physiologically realistic model which accounted for the potential adjustment in forest leaf area and related traits to future conditions. If forests fail to adjust, only 55% of climate projections predict a CO_2 increase large enough to prevent warming from causing significant drought and mortality. If forests can adjust, the percentage of favorable outcomes rises to 71%. However, uncertainty remains in whether trees can adjust rapidly and in the scatter among climate projections.

Predictive models are likewise challenged with representing the physiological response to ΔC_a and ΔT at multiple spatial (leaf–tree–stand) and temporal (short- to long-term) scales (20). Uncertainty begins at the leaf-level with stomata. Stomatal pores are the gatekeepers of terrestrial photosynthesis and transpiration, and their aperture actively adjusts to multiple external cues including C_a, D, and root zone soil water status. Most landscape-scale models predict stomatal responses from empirical functions fitted to historic conditions (21–23), but there is no guarantee these physiologically blind functions will predict a changing future with potentially acclimating vegetation (24). Acclimation of tree LA and leaf photosynthetic capacity complicates stomatal regulation, which is known to be coordinated with these internal factors (25–28). Despite these complexities, it is essential to improve the modeling of stomatal gas exchange, because instantaneous rates of photosynthesis and transpiration underlie long-term projections of NPP and stand water stress. Models also must connect soil drought to the plant stress response, and whether the response ultimately leads to mortality or adaptive acclimation.

In this paper, we combine optimality theory and established physiological mechanisms to make robust estimates of the response of trees and stands to future ΔC_a and ΔT. The proposed optimizations apply regardless of climate and C_a, meaning the basis of prediction is as valid for any future climate as it is for historic conditions. As outlined below, these optimizations were used to 1) solve stomatal regulation, 2) justify basic hypotheses for how trees acclimate LA and photosynthetic capacity to environmental conditions, and 3) control for the influence of stand structure and root depth on drought stress and mortality. The optimizations apply at different scales, but all are mechanistically connected by the central process of vascular water transport, the "functional backbone of terrestrial productivity" (29). Water supply and transport is essential to plant functioning, and its failure by stress-induced xylem cavitation limits plant gas exchange and survival (30). Threshold losses of plant hydraulic conductance on the order of 60 to 85% have been reliably linked to the risk of drought mortality (31–37).

Stomatal optimization assumed that stomatal regulation evolved to balance a trade-off between photosynthesis and transpiration-induced water stress (6, 29, 38, 39). Thus, we balance stomatal aperture to maximize the difference between relative photosynthetic gain minus the corresponding relative risk of canopy desiccation caused by transpiration-induced xylem cavitation (40, 41). This "gain–risk" optimum is calculated from commonly measured traits of photosynthetic and hydraulic capacity and the environmental conditions. The balance point solves for stomatal fluxes of water and CO_2 under any combination of environmental cues without the need for ad hoc empirical parameters. Variations in stomatal

sensitivity to water stress emerge from variation in photosynthetic and hydraulic properties. Importantly, the gain–risk calculation has been experimentally validated by successfully predicting physiological responses to C_a, D, soil moisture, and rainfall/irrigation as measured in growth chamber and plantation experiments designed to evaluate the approach (15, 36). The gain–risk concept outperformed other optimization approaches in a large-scale analysis of over 30 woody species across the world (42).

The established concept of an optimal metabolic set point for CO_2 concentration inside the leaf (C_i) leads to a hypothesis for how tree LA should be coordinated with leaf photosynthetic capacity. Under photosynthetically favorable conditions (field capacity soil, low D, and saturating light), plants tend to maintain an approximately constant C_i/C_a ratio (ca. 0.7), regardless of variation across time and space in what constitutes favorable conditions, including different C_a (3, 26, 43–45). An optimal C_i generally represents the balance or colimitation of dark vs. light reactions of photosynthesis (46, 47). Too low of a drawdown in C_i under light-saturating conditions exposes an underutilized photosynthetic capacity to light damage and energy-draining photoprotection and repair (2). The C_i/C_a set point is achieved by an optimal balance between photosynthetic capacity per LA (V_{max25} and J_{max25}) and prevailing stomatal aperture (Fig. 1A). The stomatal aperture depends in turn on the hydraulic conductance of the tree (K_{tree}, volume flow rate per soil-canopy pressure drop) per LA, a behavior captured by the gain–risk algorithm (40). A constant hydraulic conductance of root and stem system specifies the coordination between LA and photosynthetic capacity that satisfies C_i/C_a homeostasis for prevailing environmental conditions (Fig. 1B, C_i/C_a contours).

In addition to optimizing C_i/C_a, we assumed that trees optimize the return on investment (ROI) in LA (27, 48–50). Many combinations of LA and photosynthetic capacity can satisfy the C_i/C_a criterion (Fig. 1B, C_i/C_a contours), but if leaf investment scales with LA, only one pair will maximize photosynthetic returns relative to the cost of leaf production (Fig. 2C, arrow and Fig. 2B, symbols). The optimization of C_i/C_a and ROI allowed us to predict tree-level acclimation of LA and photosynthetic capacity, traits which are known to be highly responsive to environment within a species (16–18, 27). Alternatively, if trees fail to acclimate to future conditions, we were able to assess the degree of metabolic stress caused by suboptimal C_i/C_a.

Finally, the theory of ecohydrologic equilibrium (51–54) was used to scale from acclimation of single trees to adjustments at the stand scale. Over a multiyear timeframe of variable weather, the theory poses that a mature stand will maintain a demand for water that maximizes productivity but does not significantly stress or kill individual trees. Indeed, mature stands in drier habitats attain a lower
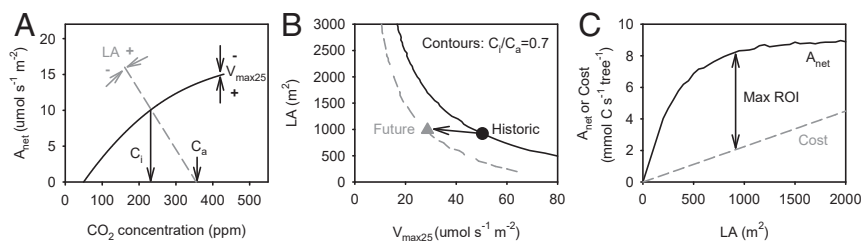
Fig. 1. Basis for modeling tree-level acclimation of LA and photosynthetic capacity (maximum carboxylation capacity, V_{max25}, coupled to electron transport capacity, J_{max25}). (A) Trees acclimate LA and V_{max25} to achieve a homeostatic ratio between leaf internal (C_i) and atmospheric (C_a) CO_2 concentrations (C_i/C_a = 0.7) under favorable site "reference" conditions. The C_i is determined by the balance between V_{max25} (V_{max25} arrows) and the stomatal conductance to CO_2 (absolute value of slope of dashed gray line). Stomatal conductance depends on LA through its effect on the tree hydraulic conductance per LA (LA arrows). (B) For each set of environmental reference conditions there are infinite combinations of LA and V_{max25} that satisfy C_i/C_a = 0.7 (solid black contour for historic conditions and gray dashed contour for future conditions), but only one LA–V_{max25} combination is optimal (historic, black circle; future, gray triangle). (C) The optimal LA–V_{max25} maximizes the ROI (Max ROI arrow), calculated as the difference between the net whole canopy assimilation (solid A_{net} curve) and leaf construction cost amortized over the GS (gray cost line).
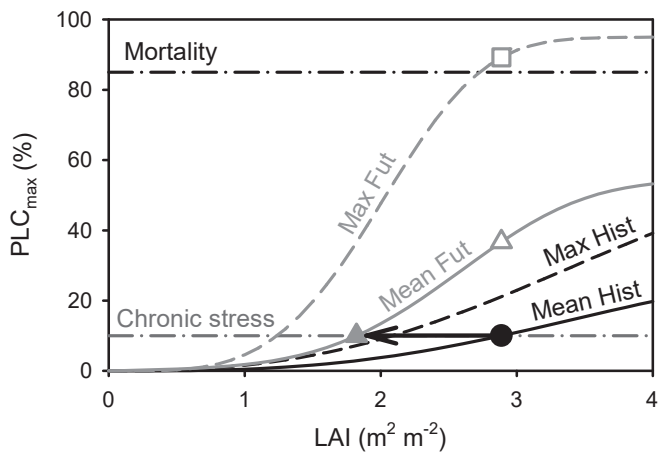
Fig. 2. Stand-level acclimation to ecohydrologic equilibrium. At equilibrium for historic conditions, the LA index (LAI) is maximized without exceeding a chronic stress threshold, defined by an average maximum percentage loss in tree hydraulic conductance over multiple GSs of variable historic weather (mean $PLC_{max} = 10$ in this study, dashed-dotted chronic stress line). The equilibrium LAI is at the intersection between the stress threshold and the "Mean Hist" PLC_{max} curve (solid black circle). Equilibrium LAI also cannot allow the PLC_{max} in any given (dry) year ("Max Hist" dashed curve) to exceed a mortality threshold (black dashed-dot mortality line, here set to $PLC_{max} = 85$; ref. 36). If the historic LAI is too high for future conditions, it will induce chronic stress (open gray triangle on "Mean Fut" curve) and possibly trigger mortality (open gray square on "Max Fut" curve). Acclimation in this case requires a reduction in LAI (black arrow) to eliminate stress (solid gray triangle). Alternatively, if the historic LAI was too low for the future, it was increased until reaching the chronic stress or mortality thresholds.

BAI and LAI than mature stands in wet habitats (54), at least up to a maximum light-limiting LAI (*ca.* 8 $m^2 \cdot m^{-2}$). We exploited this definition of sustainable carrying capacity to adjust BAI and LAI of rain-fed (no access to groundwater) mature stands of given tree size and rooting depth to weather conditions (Fig. 2). The equilibrium LAI and tree biomass was defined as the maximum possible without inducing meaningful loss in tree hydraulic conductance from xylem cavitation, as averaged over multiple growing seasons (GSs) (Fig. 2, solid circle at chronic stress threshold on historic mean PLC_{max} curve).

Ecohydrologic equilibrium allowed us to predict the stand level "acclimation" in LAI and tree biomass to future conditions. Important to the question of tree carbon storage capacity, these biomass adjustments represented sustainable, steady-state carrying capacities of a mature stand rather than potentially transient changes in growth rate. Alternatively, if stands fail to acclimate to a new equilibrium, we could quantify the consequences. If the historic LAI is too high for future conditions, average GS cavitation will become significant (Fig. 2, open triangle on future mean PLC_{max} curve) and the maximum cavitation in any given year can exceed a mortality threshold in loss of hydraulic conductance (Fig. 2, open square on future maximum PLC_{max} curve). If historic LAI is too low, the stand is nonstressed but below its maximum productivity and biomass.

This nested series of optimizations allowed us to quantify how future forests will balance the potential benefits of ΔC_a vs. the potential disadvantages of ΔT. "Forests" were modeled as monospecific stands (either a conifer or an angiosperm) of identically sized mature trees, watered only by incident precipitation. Stands were given the soil type, climate, and dominant species of 20 locations sampling the forested regions of the continental United States (2 species per location for a total of 40 stands; Dataset S1). Stands were initially acclimated to historic C_a and weather to minimize metabolic stress (Fig. 1B, symbol on historic C_i/C_a contour

at maximum ROI), and to minimize drought exposure at ecohydrologic equilibrium (Fig. 2, circle on historic mean PLC_{max} curve). We then posed the following questions about future forest responses. 1) If there is no acclimation, future ΔC_a and ΔT will drive stands out of C_i/C_a homeostasis and away from ecohydrologic equilibrium. To what extent will a ΔC_a-driven boost in NPP be compromised by a ΔT-driven rise in stress and mortality? 2) If there is stress-avoiding acclimation to future C_i/C_a homeostasis and hydrologic equilibrium, to what extent will the ΔC_a-driven boost to NPP and tree biomass be offset by a ΔT-driven reduction in NPP and tree biomass? 3) Are the projections of ΔC_a sufficiently high relative to ΔT for acclimated forests to increase NPP and tree carbon storage?

Results

The future climate (2070 to 2099) across the 20 sites projected by 6 coupled climate–Earth system models (ESM; Dataset S2) was significantly warmer, with drier air and a longer GS as compared to historic climate (1976 to 2005; *SI Appendix*, Fig. S1). Both historic and future weather included interannual fluctuations typical to each site, but the overall mean GS temperature increased by an average $\Delta T = 2.5 \pm 1.0$ °C ($\pm$ SD; RCP4.5; average $C_a = 531.9$ ppm) and $\Delta T = 4.5 \pm 1.0$ °C (RCP8.5; average $C_a = 804.0$ ppm). The average ΔT varied little across sites (under 17% of variation explained by site, ANOVA), and variation in ΔT was primarily between ESM projections (56 to 63% of variation). The mean GS D increased $27.1 \pm 12.8\%$ (RCP4.5) and $55.6 \pm 23.3\%$ (RCP8.5) relative to historic climate. The ΔT was strongly correlated with ΔD (RCP4.5, $R^2 = 0.58$, $P < 0.0001$; RCP8.5, $R^2 = 0.53$, $P < 0.0001$). There was no significant change in mean daily GS precipitation or annual precipitation, indicating no overall trend in water supply for the rain-fed stands during the GS (*SI Appendix*, Fig. S1). As a result of warming, the GS length increased an average of 6.1 and 9.6 d for RCP 4.5 and RCP 8.5, respectively. GS length increased proportionally more for sites with historically shorter GS.

Future Projections without Forest Acclimation. By definition, no acclimation to future ΔC_a and ΔT resulted in trees failing to maintain C_i/C_a homeostasis and stands falling out of ecohydrological equilibrium. Under these conditions, NPP (tree photosynthesis − tree respiration, mean annual over 30 y) increased by an approximately constant percentage across all sites, species, and climate models and showed only a slight decrease with ΔT projections within each ΔC_a regime (Fig. 3A, gray symbols). Mean NPP increased less for the representative concentration pathway (RCP) 4.5 conditions ($30.0 \pm 8.4\%$) than for RCP8.5 ($57.5 \pm 15.3\%$). Low variation in the NPP response was consistent with ΔC_a as the major NPP driver, given the variation in ΔT (Fig. 3A) and the diversity of species traits (Dataset S3). Our no-acclimation simulations meant no adjustment in tree LA or stand LAI, and as a result stand biomass and carbon storage capacity did not change. Stand transpiration (E, mean annual over 30 y) decreased slightly for futures with less warming (low ΔT) but increased above historic levels with more warming (higher ΔT; Fig. 3C).

Warmer futures (greater ΔT) induced more chronic water stress within both ΔC_a scenarios (Fig. 3D, mean $PLC_{max} > 10$ PLC_{max} stress threshold). Regionally, the highest incidence of chronic water stress was predicted for the Mountain West region of the United States, followed by Pacific Northwest and Boreal regions with the lowest incidence in the Southeast (Fig. 4 *A* and *B*).The risk of drought-induced mortality followed a different pattern, being more weakly related to average warming (Fig. 3D, red symbols exceeded $PLC_{max} = 85$ in at least one year of 30), and being highest in the Southeast and Mountain West, lower in the Boreal, and least in the Pacific Northwest (Fig. 4 *C* and *D*). The percentage of stands exceeding the mortality threshold was
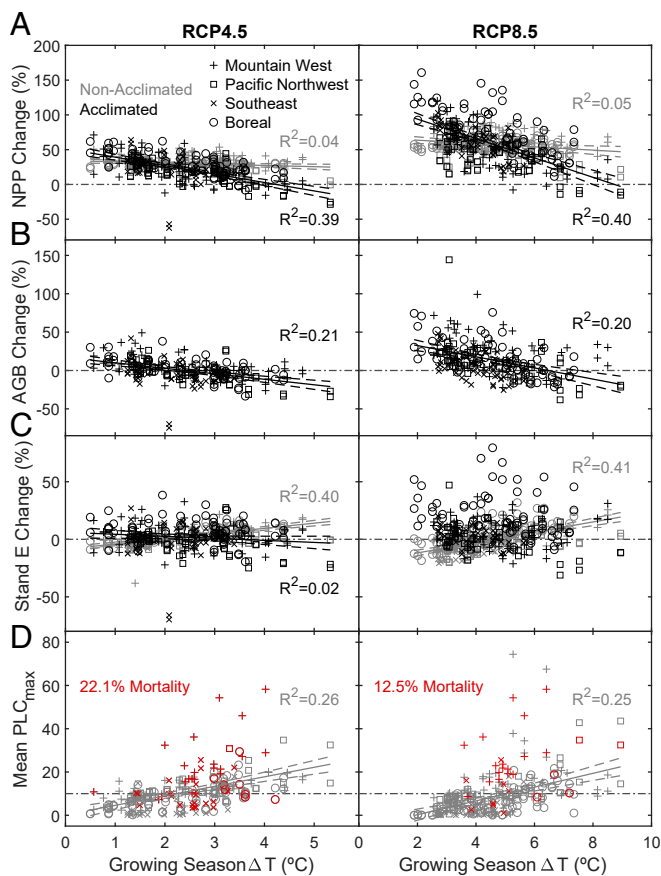
Fig. 3. Stand responses to the increase in GS temperature (ΔT) at 2 elevated atmospheric CO_2 concentrations, RCP4.5 (ΔC_a = 177 ppm, *Left*) and RCP8.5 (ΔC_a = 449 ppm, *Right*). Nonacclimated stands are in gray and acclimated stands are in black. Symbols indicate regions: Mountain West, +; Pacific Northwest, □; Southeast, ×; Boreal, ○. Regressions (solid lines) were highly significant (n = 240, P < 0.001; 95% confidence intervals, dashed lines). (*A*) The percentage change (all percentages relative to historic) in mean annual NPP. (*B*) Percentage change in AGB. (*C*) Percentage change in mean annual stand transpiration (*E*). (*D*) Mean maximum percentage loss in soil-to-canopy tree conductance at the end of the GS (mean PLC_{max}). Dashed-dotted horizontal line is the 10% chronic stress threshold (Fig. 2). Red symbols are simulations in which maximum PLC_{max} exceeded the mortality threshold (PLC_{max} = 85; Fig. 2) in at least one year, with the percentage of total simulations (n = 240 per RCP CO_2 concentration) indicated. Acclimated stands by definition did not exceed either threshold.

greater in the moderate (RCP4.5, 22.1%) vs. the high (RCP8.5, 12.5%) ΔC_a scenario (Fig. 3*D*), as was average chronic stress. Greater stress for RCP4.5 was consistent with its having a lower ΔC_a relative to the average ΔT ($\Delta C_a/\Delta T$ = 71 ppm·°C^{-1}) compared to RCP8.5 ($\Delta C_a/\Delta T$ = 100 ppm·°C^{-1}).

Trees experienced greater "metabolic stress" as indicated by a reduced mean annual C_i/C_a (weighted by the photosynthetic rate) relative to historically acclimated stands (*SI Appendix*, Fig. S2). The C_i/C_a declined with greater mean annual PLC_{max} (linear regression, r = −0.46 and P < 0.0001), meaning that the greater warming associated with water stress (Fig. 3*D*) also contributed to increased metabolic stress. Both metabolic and water stress occurred in warmer futures where historic LAI was too high to maintain ecohydrological equilibrium under future conditions (*SI Appendix*, Fig. S3).

Future Projections with Acclimation. Acclimation to future ΔC_a and ΔT required changing tree LA and photosynthetic capacity to maintain C_i/C_a homeostasis and maximize ROI (i.e., no metabolic

stress) and adjusting stand biomass to stay in ecohydrologic equilibrium (i.e., no long-term drought stress). Under these conditions, NPP declined strongly with climatic warming within each ΔC_a scenario (Fig. 3*A*, black symbols). Less warming allowed for greater NPP fertilization compared to nonacclimated stands. In contrast, under strong warming scenarios our model predicted a much weaker NPP increase, and in some instances a decline in NPP, relative to historic levels (Fig. 3*A*). Biomass carrying capacity mirrored the NPP response (Fig. 3*B*). The weakest NPP and biomass responses were seen for RCP4.5 with its smaller $\Delta C_a/\Delta T$ ratio as compared to RCP 8.5. The acclimation to ecohydrological equilibrium eliminated the increase in stand E with warming: instead E either declined with warming (RCP4.5; Fig. 3 *C*, *Left*) or showed no trend (RCP8.5; Fig. 3 *C*, *Right*).

At the tree scale, our acclimation hypothesis predicted an increase in tree LA and a decrease in V_{max25}; however, the response varied substantially (Fig. 5*A*) and depended on ΔC_a, ΔT, and factors specific to site and species. The adjustments were greater for the higher ΔC_a scenario (Fig. 5*A*). For RCP8.5, LA increased by 21.5 ± 19.5% and V_{max25} decreased −28.7 ± 13.3%, whereas for RCP4.5, LA increased by 11.8 ± 9.4% and V_{max25} decreased −19.9 ± 8.6% (Fig. 5*A*, $\Delta C_a\Delta T$). Within ΔC_a scenario, there was a trend for less adjustment of LA and larger decrease in V_{max25} with greater ΔT (*SI Appendix*, Fig. S4 *A* and *B*).

At the stand level, the adjustment to ecohydrologic equilibrium resulted in little change in average LAI and BAI for RCP4.5 and an increase for RCP8.5 (Fig. 5*B*). However, the individual responses varied substantially depending on ΔT: Less warming resulted in more LAI and BAI relative to historic levels, while greater warming resulted in reductions (*SI Appendix*, Fig. S4 *C* and *D*). This pattern drove the trend for tree NPP and biomass to decrease with ΔT (Fig. 3 *A* and *B*). Warmer futures where hydrologic equilibrium required reductions in stand biomass were the same futures inducing stress in nonacclimating stands (Fig. 3*D*).

The Conflict between ΔC_a and ΔT. The tension between the advantages of higher C_a vs. the disadvantages of greater warming as seen within future climate projections ($\Delta C_a\Delta T$, Figs. 3–5) were also evident by comparing the mean future response (Fig. 6, $\Delta C_a\Delta T$) with simulations that uncoupled C_a from climate (Fig. 6, ΔC_a, ΔT). In nonacclimating stands (Fig. 6, open bars), where tree biomass was fixed by definition, raising C_a to future levels without any warming increased average NPP (Fig. 6*A*, ΔC_a). There was no chronic stress or mortality (Fig. 6*C*, ΔC_a) as a result of a decrease in stand transpiration (Fig. 6*D*). Adding warming maintained the potential NPP increase but induced stress and mortality (Fig. 6*C*, $\Delta C_a\Delta T$) along with a rise in average stand transpiration (Fig. 6*D*, $\Delta C_a\Delta T$). A warm future without elevated C_a resulted in either no increase in average NPP (RCP4.5; Fig. 6*A*, ΔT) or an NPP decline (RCP8.5; Fig. 6*A*, ΔT) and triggered a major spike in chronic water stress and mortality (Fig. 6*C*, ΔT) that was associated with a further increase in stand transpiration (Fig. 6*D*, ΔT).

Acclimation accentuated the CO_2 fertilization of NPP and increased the carrying capacity of tree biomass in the absence of warming but sacrificed productivity and biomass accrual to eliminate warming-induced stress and mortality (Fig. 6, gray bars). Compared to nonacclimated stands, acclimation resulted in higher NPP for elevated C_a without warming and greater tree biomass (Fig. 6 *A* and *B*, ΔC_a) but caused lower NPP and nearly neutral biomass with both warming and increased C_a (Fig. 6 *A* and *B*, $\Delta C_a\Delta T$). Warming without elevated C_a resulted in a major reduction in NPP and tree biomass (Fig. 6 *A* and *B*, ΔT) to avoid stress. The absence of stress and mortality in acclimated stands was associated with maintenance of average stand transpiration across all scenarios, consistent with ecohydrologic equilibrium (Fig. 6 *C* and *D*).

Trends in the adjustment of LAI and BAI (Fig. 5*B*) to ecohydrological equilibrium explained trends in the indicators of
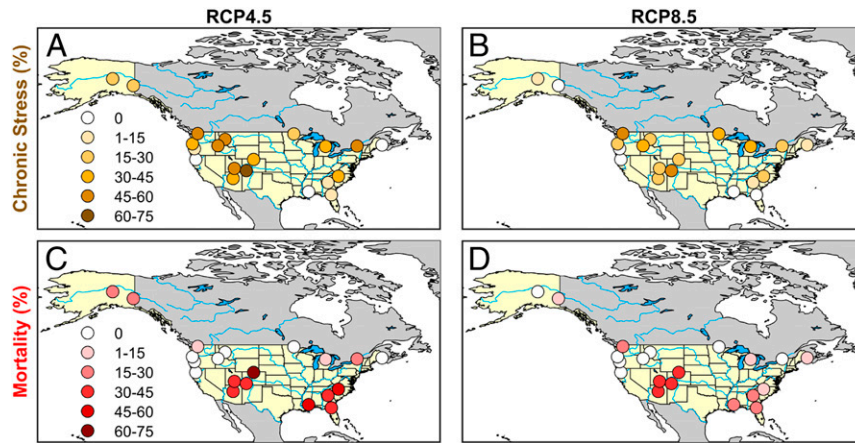
Fig. 4. Regional distribution of chronic hydraulic stress and mortality for nonacclimated stands. Chronic hydraulic stress (orange-toned circles) indicated as the percentage of simulations per site ($n = 12$, 6 climate models and 2 species per location) exceeding the chronic stress threshold in average percentage loss of hydraulic conductance (Fig. 2, mean $PLC_{max} = 10$) over a 30-y period. Mortality (red-toned circles) is indicated as percent of simulations per site exceeding the hydraulic mortality threshold in any year (Fig. 2, max $PLC_{max} > 85$). Darker symbols represent higher levels of stress as labeled. (*A*) Chronic stress for RCP4.5 CO_2 concentration. (*B*) Chronic stress for RCP8.5. (*C*) Mortality for RCP4.5. (*D*) Mortality for RCP8.5.

stress and mortality in nonacclimated stands. When acclimation to equilibrium drove a reduction in LAI and BAI, as in the warming only situation (Fig. 5*B*, ΔT), nonacclimated stands had LAI in excess of equilibrium and stress resulted (*SI Appendix,* Fig. S3). When acclimation drove an increase in LAI and BAI (Fig. 5*B*, ΔC_a, $\Delta C_a \Delta T$), nonacclimated stands had an excess water supply and experienced no stress (*SI Appendix,* Fig. S3). At the tree level, acclimation to higher C_a without warming predicted lower V_{max25} and greater tree LA, much as reported for higher C_a with warming (Fig. 5*A*). In contrast, acclimation to warming without elevated C_a required little change in average V_{max25} and a reduction in tree LA (Fig. 5*A*).

We used the model to predict $\Delta C_a / \Delta T$ thresholds that were necessary to counteract the negative effects of future warming. If forests do not acclimate to climate change, the C_a must rise at least 89 ppm for every 1 °C of warming to avoid chronic water stress (Fig.

7*A*; gray 10 mean PLC_{max} contour), and a much steeper 332 ppm·°C^{-1} to prevent mortality (Fig. 7*A*, dashed 10% mortality contour). Mean $\Delta C_a / \Delta T$ projections for both ΔC_a scenarios did not meet these stress thresholds (Fig. 7*A*), hence the negative effects of warming as predicted for nonacclimating stands (Figs. 3*D* and 4). As noted, the $\Delta C_a / \Delta T$ for RCP4.5 (71 ppm·°C^{-1}) was further below the thresholds than RCP8.5 (100 ppm·°C^{-1}), explaining the greater incidence of stress and mortality in the RCP4.5 projections (Figs. 3*D* and 4).

If forests do acclimate to climate change, C_a must rise at least 31 ppm for every 1 °C of warming for C_a fertilization of NPP to occur (Fig. 7*B*, zero NPP contour), and 67 ppm·°C^{-1} for the carrying capacity of tree biomass to increase (Fig. 7*C*, zero biomass contour). Average $\Delta C_a / \Delta T$ projections for both RCP4.5 and 8.5 were above the C_a fertilization threshold (Fig. 7*B*) and at or above the biomass accrual threshold (Fig. 7*C*). The greater $\Delta C_a / \Delta T$ for RCP8.5 was more hospitable to future forests, resulting in a greater boost in NPP and biomass under RCP8.5 projections (Figs. 3, 6, and 7). The considerable uncertainty in warming and C_a rise translated into NPP uncertainty ranging from over +75% (Fig. 7*B*, RCP8.5 outliers) to 0% (Fig. 7*B*, RCP4.5 outliers) and biomass uncertainty from over +35% (Fig. 7*C*, RCP8.5 outliers) to below −25% (Fig. 7*B*, RCP8.5 outliers). Overall, the degree of stress or strength of CO_2 fertilization and tree carbon storage was quantifiably sensitive to the climatic $\Delta C_a / \Delta T$ ratio.

Discussion

Our fundamental question was whether ΔC_a and acclimation can compensate for ΔT-induced impacts on US forests. Our sensitivity analysis did indeed identify compensating $\Delta C_a / \Delta T$ thresholds that neutralized climate change impacts on stand stress, mortality, NPP, and biomass. Acclimation did succeed in avoiding ΔT-driven stress and mortality through a reduction in stand LA. However, for this same reason acclimation cannot compensate for ΔT-driven declines in stand NPP and biomass. The answer to our question thus depends on whether future climate produces $\Delta C_a / \Delta T$ ratios in excess of compensating thresholds for acclimating stands. If NPP and biomass are both to increase for future stands, there must be at least a 67 ppm increase in C_a for every °C (zero contour in Fig. 7*C*). The sampled climate projections spanned this threshold. Over both ΔC_a scenarios, 71% of the projections predicted an increase in biomass and 29% predicted a decrease. If stands fail to acclimate,
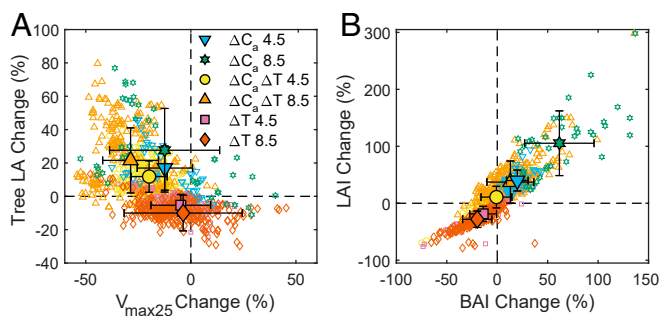

Fig. 5. Acclimation at the tree and stand scale to 6 future scenarios of elevated atmospheric CO_2 (ΔC_a) and warming of the GS (ΔT). Scenarios by color: ΔC_a 4.5, historic climate with RCP4.5 atmospheric CO_2 concentration (blue downward triangle, $n = 40$); ΔC_a 8.5, historic climate with RCP8.5 C_a (green star, $n = 40$); $\Delta C_a \Delta T$ 4.5, future RCP4.5 weather and C_a (yellow circle, $n = 240$); $\Delta C_a \Delta T$ 8.5, future RCP8.5 weather and C_a (orange upward triangle, $n = 240$); ΔT 4.5, future RCP4.5 weather and historic C_a (pink square, $n = 240$); ΔT 8.5, future RCP8.5 weather and historic C_a (vermillion diamond, $n = 240$). Open symbols are individual simulations, and solid symbols are simulation means (SD bars). (*A*) Tree-level acclimation by percentage change (all percentages relative to historic) in maximum carboxylation rate (V_{max25}, coupled to electron transport capacity, J_{max25}) and percentage change in tree LA. (*B*) Stand-level adjustment by percentage change in stand basal area (BAI) and percentage change in LA index (LAI) as required to satisfy ecohydrologic equilibrium.
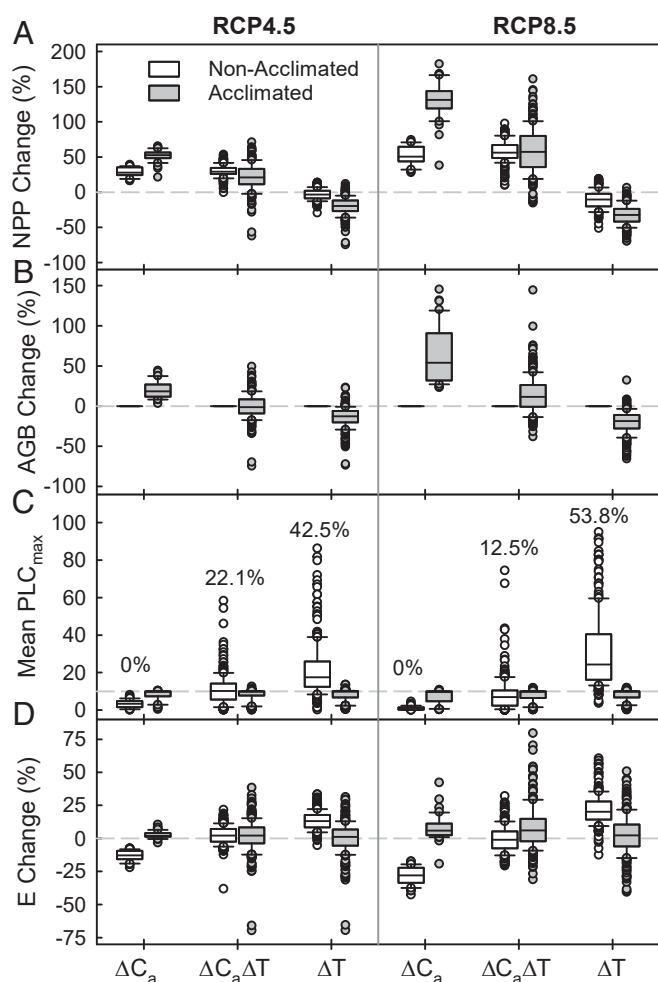
Fig. 6. Response of stands to 6 future scenarios of elevated atmospheric CO_2 (ΔC_a) and warming of the GS (ΔT). (*Left*) RCP4.5 ΔC_a. (*Right*) RCP8.5. The ΔC_a treatment (bottom axis) is future CO_2 enrichment with historic weather ($n = 40$ simulations); $\Delta C_a \Delta T$ is the future CO_2 and weather ($n = 240$); ΔT is future weather with historic CO_2 concentration ($n = 240$). Box and whisker plots characterize the distribution of individual simulations within each scenario (boxes = 25th to 75th percentile with median line; whiskers = 10th and 90th percentiles; symbols = remainder). Nonacclimated stands are open boxes, acclimated stands are gray. (*A*) Percentage change in NPP (all percentages relative to historic). (*B*) Percentage change in AGB. (*C*) Mean GS percent loss in tree hydraulic conductance (Mean PLC_{max}). Percentages above the open nonacclimated simulations are the percent of simulations that reached the mortality threshold (Fig. 2, $PLC_{max} \geq 85$) at least once in the 30-y simulation period. (*D*) Percentage change in stand transpiration (E).

the bar is raised to a compensating $\Delta C_a / \Delta T$ threshold of 89 ppm·°C^{-1} to avoid water stress (10 PLC contour in Fig. 7*A*). In this case, only 55% of the $\Delta C_a / \Delta T$ projections were sufficiently high to compensate for ΔT-induced stress.

The negative effects of warming acted in our model primarily through the increase in *D* (*SI Appendix*, Fig. S1). Higher *D* increased stand transpiration relative to incoming precipitation and root zone storage, pushing nonacclimating stands out of ecohydrologic equilibrium and causing water stress and mortality. Although the gain–risk stomatal algorithm typically responds to a rise in *D* by partial stomatal closure, the closure is usually not sufficient to prevent an increase in transpiration (40), which increases the rate of soil drying (8). If root zone withdrawals exceed precipitation inputs, soil moisture declines and xylem pressures become more negative, causing cavitation to accumulate

during the GS. The gain–risk stomatal algorithm ensured that cavitation developed in a controlled manner, allowing the plant to exploit its capacity for water extraction while avoiding complete hydraulic failure (at 100 PLC_{max}) and instant desiccation. Unless rainfall intervenes, cavitation will eventually rise above the mortality threshold of 85 PLC_{max}. This stress cycle was more gradual in fine-textured soils where pressure dropped more gradually with drying, but it could develop over a matter of days in coarser soils where pressures plummet abruptly as large soil pores empty. In either case, the nonlinear dynamics of water stress made its onset highly sensitive to the timing of GS rainfall and the *D* regime, both which varied annually in our 30 y simulations and created considerable interannual variation in water stress.

The tipping-point nature of stand water stress resulted in the development of increasingly skewed distributions in mean PLC_{max} (e.g., Fig. 6*C*, outliers) as warming caused more stands to transition to a stressed state. Because mortality can be triggered by a single dry year, it was stochastic and only loosely coupled to chronic stress and ΔT, which tracked 30-y average conditions. This model behavior supports the importance of subtle changes in drought timing, atmospheric *D*, and stand density as major drivers of future mortality (8, 55–57). The predicted vulnerability of the southeastern United States to future stress (Fig. 4) is consistent with the tree ring record showing sensitivity of these forests to seasonal drought and elevated *D* (58, 59).

Water stress was associated with low C_i/C_a, or "metabolic" stress caused by chronic reductions in stomatal aperture in response to high *D* and drier soil. Whereas the consequences of water stress were quantified in terms of reduced photosynthesis, increased cavitation, and loss of hydraulic conductance, additional downsides of operating at overly low C_i are more difficult to calculate. Beyond the reduction of gas exchange caused by stomatal closure and cavitation, for lack of definitive information we did not subtract any additional effects of stress and putative mortality on NPP. In particular we assumed full hydraulic recovery between GSs, erasing the drought legacy between GSs. For this reason, our NPP and biomass estimates for nonacclimated stands under stress-inducing conditions represented potential maxima.

The acclimation scenario, which minimized metabolic and water stress averaged over a 30-y period of variable conditions (Figs. 1 and 2), produced realistic trends in tree LA, V_{max25}, and stand LAI for a variety of climatic scenarios (Fig. 5). Direct comparison with experiments is complicated because the degree of acclimation as we defined it was not always assessed, and experiments combine changes from growth rate and ontogeny with adjustments in steady-state carrying capacity. FACE studies (3, 4) which raise C_a (to *ca.* 550 to 580 ppm) without warming generally compare favorably with simulation results for ΔC_a at RCP4.5 ($C_a = 532$ ppm). The LAI of FACE tree stands increased +21% on average (range +43% to −8%; refs. 3 and 4) within the wide range of our simulations (+13% to +94%, mean 40%; ΔC_a 4.5; Fig. 5*B*). LA per tree sapwood area also increased with elevated C_a in a number of studies (27, 60), which is consistent with the simulated increase in tree LA (Fig. 5*A*, ΔC_a 4.5). The trend for greater LAI in elevated C_a experiments is generally accompanied by no apparent change in C_i/C_a and a decline in V_{max25} in trees (*ca.* −6% for FACE trees; refs. 3, 26, 44, and 45). This result was consistent with acclimation to a constant reference-condition C_i/C_a and the simulated decline in V_{max25} (−38% to +10%, mean −12%; Fig. 5*A*, ΔC_a 4.5). Aboveground tree biomass increased 28% on average in FACE studies (3) with considerable variation, which is consistent with our average +21% increase (range +3% to +44%; Fig. 6*B*, ΔC_a 4.5). Variation between experiments is a prominent theme in elevated CO_2 studies (3, 4) and is consistent with the highly variable results of the simulations (Fig. 6). Clearly, the acclimation response to a specific C_a change depends on many other factors, climate and species traits being among them.
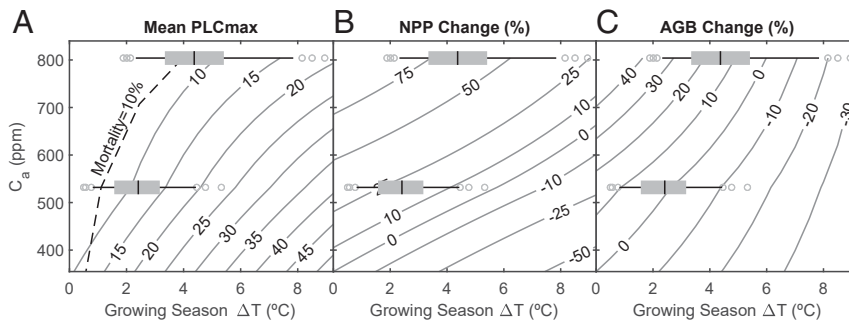
Fig. 7. Competing effects of atmospheric CO_2 enrichment (C_a) and warming of the GS (ΔT). Contour lines for each response variable were obtained from linear regressions with ΔT (based on historic, RCP4.5, and RCP8.5 weather) at each of 3 C_a (historic, RCP4.5, and RCP8.5; $n = 520$ per C_a). Superimposed are ΔT distributions for an RCP4.5 future (lower box and whisker, $n = 240$) and an RCP8.5 future (upper box and whisker, $n = 240$; boxes = 25th to 75th percentile with median line; whiskers = 10th and 90th percentiles; symbols = remainder). (*A*) Stress in nonacclimated stands indicated by contours of mean PLC_{max} (gray) and the 10% mortality contour (dashed black; 10% of simulations reaching $PLC_{max} \geq 85$). (*B*) NPP in acclimated stands indicated by contours of percentage change (all percentages relative to historic) of acclimated stands. (*C*) AGB in acclimated stands indicated by contours of percentage change.

Fewer experiments have addressed acclimation to warming in the absence of elevated C_a and in the presence of rising D and a constrained soil water supply (*SI Appendix*, Fig. S1). Warming treatments either increase or decrease V_{max25} (19, 61), which was consistent with the highly variable V_{max25} acclimation predicted by our model (Fig. 5*A*, ΔT). Area of individual leaves generally decreases in plants grown under higher D (62, 63), and LA per sapwood area tends to decrease (27, 64–67, but see ref. 68), and both observations are consistent with our prediction of reduced tree LA under warmer and drier air (Fig. 5*A*). Tests of the ecohydrological equilibrium concept generally support the simulated trend toward reduced LAI, BAI, and above-ground biomass in regions with warmer and drier air (Fig. 5*B* and ref. 54). Overall, the acclimation of traits required by the model is within the observed range of responses, indicating that at least some degree of acclimation to climate change will continue to happen.

The degree of C_a fertilization, as predicted by increases in acclimated stand NPP (Figs. 3, 6, and 7), was generally consistent with trends from experiments. The relatively constant percentage boost of NPP from C_a fertilization, regardless of species or site, was also reported across a range of FACE sites (3, 4). Some studies report a nutrient-limited saturation of C_a fertilization after several years or altered nutrient cycles (69–72). Although we did not model nutrient limitation, the V_{max25} per ground area either remained approximately constant or even declined in our simulations (*SI Appendix*, Fig. S5, $\Delta C_a \Delta T$), suggesting that this proxy of nitrogen demand was not likely to limit NPP as long as historic N availability is sustained. Importantly, we modeled NPP as annual production of fixed carbon (canopy photosynthesis minus plant respiration), whereas measured NPP is based on tracking the fate of this carbon in harvestable biomass, which is challenging below ground and excludes losses to herbivory, volatiles, exudates, and mycorrhizal uptake. The 2 NPP estimates often do not track each other owing to the difficulty of closing the plant's carbon budget (3, 4, 14, 73).

Our model simulations were structured to focus on the response of a given species to changing C_a and climate, with acclimation limited to LA, V_{max25}, and LAI–BAI. Although species differed considerably in their photosynthetic and hydraulic traits (Dataset S3), they all responded in a similar manner to a particular shift in climate and C_a. At a given site, the response was more sensitive to variation between the 6 ESM weather projections rather than the 2 species tested (e.g., for NPP % change "site" explained 21% and 40% of variance for RCP4.5 and RCP8.5, respectively, "species" explained 5% in both RCP scenarios, and "ESM" 70% and 50% of variance for RCP4.5 and RCP8.5, respectively; $P < 0.001$, ANOVA). The differences between species would become much more important if climate change was accompanied by a change in

species composition at a site, rather than just the response of a given species. We also did not attempt to model acclimation in other traits besides LA, V_{max25}, and LAI–BAI, chiefly because there was less known about their plasticity and spatial-temporal variation (52, 74, 75). Acclimation of other traits can be incorporated as their plasticity and adaptive significance becomes established. Species turnover and a wider sphere for acclimation could have a major impact on predictions of future forest function.

Uncoupling C_a fertilization from warming quantified the critical balance between these often opposing influences on stand function. As long as there is sufficient rise in C_a, it appears to offset mortality and loss of productivity associated with the rise in T (and associated rise in D) in our model simulations. Our results support previous modeling which indicated a pronounced reduction in warming-induced mortality risk caused by rising C_a (76, 77). In our case, elevated C_a dropped mortality (simulations reaching $PLC_{max} \geq 85$) from 43 to 22% for RCP4.5 and from 54 to 13% for RCP8.5 (Fig. 6*C*). Mortality was predicted to be especially sensitive to warming at lower C_a, requiring very steep increases in C_a to compensate (Fig. 7*A*, dashed mortality contour). This resulted in greater projected mortality for the moderate RCP4.5 ΔC_a scenario (22%) vs. the high ΔC_a one (13% for RCP8.5). High sensitivity at low C_a is also consistent with recent incidence of forest mortality worldwide (9, 78). The extent of C_a fertilization for acclimated and nonstressed forests was more uniformly sensitive to warming, requiring *ca.* 31 ppm·°C^{-1} to just offset warming-induced productivity loss. The greater the $\Delta C_a/\Delta T$ ratio, the greater the C_a fertilization, as exemplified by the NPP comparison of RCP8.5 (100 ppm·°C^{-1}, +58.4% NPP at mean ΔT) vs. RCP4.5 (71 ppm·°C^{-1}, +21.6% NPP). The same trend was seen for the C_a-stimulated increase in stand biomass, although a higher threshold of 67 ppm·°C^{-1} was required (Fig. 7*C*). Staying above these $\Delta C_a/\Delta T$ ratios would insure C_a fertilization and increased tree carbon storage to potentially mitigate the C_a rise from emissions.

Critically, the benefits of CO_2 fertilization, even for acclimating forests, are not guaranteed in a much hotter world. Uncertainty in ΔT and C_a meant that NPP could go up or stay unchanged, and tree biomass could go up or down depending on ΔT and C_a projections (Fig. 7 *B* and *C*). The $\Delta C_a/\Delta T$ thresholds of Fig. 7 are specific to rain-fed and water-limited forests of the United States with LAI mostly below 3.5 (*SI Appendix*, Fig. S5), and facing an essentially precipitation neutral future (*SI Appendix*, Fig. S1). However, the consequences of even small shifts in the balance between rising C_a and rising T can apply globally. The $\Delta C_a/\Delta T$ ratio may decrease with latitude, given that C_a rises fairly uniformly (79) while ΔT increases more at higher latitudes (80). A lower boreal $\Delta C_a/\Delta T$ (although not seen in our US-limited sample; *SI Appendix*, Fig. S1) would result in lower CO_2 fertilization

and biomass increase, a speculation that is consistent with boreal forests showing a limited growth response to warming (11, 81). By the same logic, tropical forests exposed to the highest $\Delta C_a/\Delta T$ should absorb and store more carbon, at least up to a light-limiting threshold. This agrees with at least some modeling that shows significant tropical CO_2 fertilization (82) and strong resilience to potentially negative effects of warming (77), although this may be modified by declines in precipitation observed in some climate models (83–85).

The main advance in our modeling approach was to constrain a mechanistic plant hydraulic–gas exchange model with optimality principles operating at a hierarchy of scales from leaf to forest. In some form, the concept could be scaled up to replace the empirical approach generally utilized in land surface models and ESMs, particularly with the increasing prevalence of demographic vegetation models (20, 28, 86). These models face the enormous challenge of integrating basic plant ecophysiology with potentially critical impacts of fire regime, land use, soil biogeochemistry, pathogen and pest activity, and the like. Our results provide an important step forward in projecting the future of Earth's forests in the 21st century.

Methods

Sites, Species, and Stands. We compared historic vs. future climate scenarios at 20 locations in 4 forested regions across the United States: Pacific Northwest, Mountain West, Boreal, and Southeast (Dataset S1 and *SI Appendix*, Fig. S6). Two monospecific stands were simulated per location, the species being a regionally abundant conifer or diffuse porous angiosperm (Table 1). Trees were uniformly spaced and of mature size with equal diameter at breast height (DBH) and height to standardize for demography and biomass at ecohydrologic equilibrium. Four to 6 locations were selected per forested region that 1) were within the focal species range (Table 1 and ref. 87), 2) had a nearby weather station with at least 13 y of hourly data for the variables of interest accessible through MesoWest (https://mesowest.utah.edu; Dataset S1 and ref. 88), and 3) covered a wide spatial and environmental range within the region (Dataset S1 and *SI Appendix*, Fig. S6). Soil texture for each location was obtained from the US Department of Agriculture Soil Survey Database (89).

ESM Weather Projections Selection. We used climate from 6 coupled climate–ESMs from a sample of 30 in the Coupled Model Intercomparison Project Phase 5 (CMIP5) (90) to force our forest model and estimate changes in temperature and precipitation between historic (1976 to 2005) and future (2070 to 2099) periods. The 30 ESM sample (Dataset S2) met the following model output criteria: 1) available through the Centre for Environmental Data Analysis (Natural Environment Research Council, https://www.ceda.ac.uk/); 2) included historic, RCP4.5 (91, 92), and RCP8.5 (93) simulations; and 3) included daily air surface temperature and precipitation for the historic and future 30-y periods. We used data from the first model realization (r1i1p1). For each ESM+RCP+location combination we calculated the delta change in mean annual temperature (ΔMAT) and percent change in mean annual precipitation (MAP%) and graphed them against each other. The changes were studentized (subtracting the mean and dividing by the SD per RCP scenario) to give each location and scenario equal weight in model comparison. We selected the 2 mean ESMs that were graphically closest on average to the overall mean ΔMAT and mean MAP%, and 4 extreme ESMs closest on average to the following extremes: hot–dry (maximum ΔMAT, minimum MAP%), cool–dry (minimum ΔMAT, minimum MAP%), hot–wet

(maximum ΔMAT, maximum MAP%), and cool–wet (minimum ΔMAT, maximum MAP%). As a result, the 6 ESMs selected (Dataset S2) covered a wide range of ΔMAT and MAP%, both across all sites (*SI Appendix*, Fig. S7) and within regions (*SI Appendix*, Fig. S8). Selected ESMs were from different research groups and used different oceanic, atmospheric, and vegetation submodels (Dataset S2).

Weather Generation. The hourly weather data required by our forest model (precipitation, air temperature, wind speed, solar radiation, and atmospheric D) was simulated with AWEGEN (Advanced Weather Generator; refs. 94 and 95). To obtain the parameters for weather generation, AWEGEN was "trained" on hourly weather records for each location (minimum of 13 y) and on annual precipitation records from 1976 to 2005 (National Weather Service, https://www.ncdc.noaa.gov, or 4- × 4-km gridded PRISM data, http://prism.oregonstate.edu). Once trained, AWEGEN was used to generate 35-y historic time courses (including a 5-y burn-in period) with the interannual (AR1) precipitation regime model activated (94). The 35 simulated years incorporated the interannual variation representative of each site. Future weather was generated by modifying AWEGEN parameters according to the climate change shifts from the 6 ESMs (the factor change in precipitation and delta change in temperature; refs. 94 and 96). The AWEGEN program simulated 35 y of future hourly weather, with interannual variation, for each of the 6 ESMs and 2 ΔC_a scenarios per site. Simulations assumed constant atmospheric CO_2 concentrations (C_a) over the 30-y periods. Historic C_a was set to 354.8 ppm, which is the mean annual concentration for 1976 to 2005 (Earth System Research Laboratory, National Oceanic and Atmospheric Administration, https://www.esrl.noaa.gov/). Future C_a was set to the mean of the 3 decadal values (2070 to 2100) from the RCP4.5 (531.9 ppm) and RCP8.5 (804.0 ppm) scenarios (RCP Database 2009, https://www.iiasa.ac.at/web-apps/tnt/RcpDb/dsd?Action=htmlpage&page=welcome).

GS length was estimated from annual plots of cumulative thermal degree days above 5 °C (97) from February 1. We determined the start and end day of the GS from the intersections of a 3-line best fit to the annual time course of cumulative degree days (*SI Appendix*, Methods S1 and Fig. S9).

Model Simulations. The model (36, 40) was parameterized with species traits from the literature (Dataset S3). Species-specific (nonplastic) inputs included leaf hydraulic conductance per LA, leaf width, rooting depth, and xylem vulnerability to cavitation curves for root, stem, and leaves (leaf and root curves were not available for white spruce or the leaf curve for aspen; these were replaced with the stem curves; Dataset S3). Cavitation was assumed irreversible during the GS (36) and quantified by the accumulated loss of soil-canopy hydraulic conductance by season's end (PLC$_{max}$). Tree hydraulic conductance was fully restored between GSs. If model parameters were obtained from more than one study per species we used the mean value (or fit a vulnerability curve to pooled data). Tree height was calculated from mature DBH using the Greenhill equation with a safety factor of 4.66 (98). The rhizosphere soil resistance, averaged from field capacity to the water extraction limit, was set to 50% of soil–canopy hydraulic resistance (15, 36, 99).

Literature values for the plastic traits, tree LA and photosynthetic capacity (V_{max25} and corresponding $J_{max25} = V_{max25} \cdot 1.67$; ref. 100), were used to estimate species-specific values for the hydraulic conductance of the mature tree's root and stem network (K_{wood}, root:stem components in 1:2 ratio) and the cost of leaf production amortized over the GS (moles $CO_2 \cdot s^{-1} \cdot m^{-2}$ LA). Species-specific estimates of K_{wood} and leaf cost assumed species-specific historic "reference" environmental conditions (i.e., where $C_i/C_a = 0.7$; Fig. 1) which were obtained by averaging the location-specific reference conditions for the species. Location-specific reference conditions were defined by field capacity soil, elevation, and mean atmospheric parameters (solar radiation, air temperature, D, and wind speed) for clear sky (cloudiness ≤10%) hours 0900 to

Table 1. Selected focal tree species

Region	Species	Family	Common name	Type	Leaf habit
Boreal	*Betula papyrifera* Marsh.	Betulaceae	Paper birch	Angiosperm	Deciduous
	Picea glauca (Moench) Voss	Pinaceae	White spruce	Conifer	Evergreen
Mountain West	*Populus tremuloides* Michx.	Salicaceae	Trembling aspen	Angiosperm	Deciduous
	Pinus ponderosa Douglas ex C.Lawson	Pinaceae	Ponderosa pine	Conifer	Evergreen
Pacific West	*Populus trichocarpa* Torr. & A.Gray ex Hook	Salicaceae	Black cottonwood	Angiosperm	Deciduous
	Pseudotsuga menziesii (Mirb.) Franco	Pinaceae	Douglas fir	Conifer	Evergreen
Southeast	*Liriodendron tulipifera* L.	Magnoliaceae	Yellow poplar	Angiosperm	Deciduous
	Pinus taeda L.	Pinaceae	Loblolly pine	Conifer	Evergreen

1159 of the first quarter of every GS for the 30 y of simulation (Dataset S4). The K_{wood} was set to achieve C_i/C_a homeostasis for species' LA and V_{max25} (Fig. 1*B*, historic curve and symbol). The cost of leaf production (Fig. 1*C*, dashed line) was set to maximize ROI at the species' LA based on the modeled rise in tree net photosynthesis (integrated over sun and shade layers; ref. 36) as LA was increased along the $C_i/C_a = 0.7$ contour (Fig. 1*C*, solid A_{net} curve). Species K_{wood} and leaf cost were then used to determine location-specific LA and V_{max25} (and corresponding J_{max25}) for site-specific reference conditions. Acclimation to future conditions adjusted the LA+V_{max25} setting to satisfy C_i/C_a homeostasis and ROI maximization for the future reference conditions assuming no change K_{wood} or leaf cost (Fig. 1*B*, future curve and symbol). Species traits other than LA and photosynthetic capacities were not altered (i.e., not acclimated) other than by standard temperature responses of hydraulic conductance (via water viscosity), photosynthesis (100–102), and respiration (103).

Tree LA and stand BAI were used to determine stand-level LA per ground area (LAI). This allometric LAI was converted to an optical canopy LAI as typically measured with hemispheric canopy photographs (104). The optical LAI was used to partition sun and shade layers of the canopy (36, 105).

Beneath a 2-cm rootless surface layer, the root zone was divided into 5 soil layers of equal root biomass (36). The fraction of total root biomass above depth d (in centimeters) was given by $1 − B^d$, where the extinction coefficient B ($0 < B < 1$) determined the maximum root system depth (Rd = d yielding 99.5% root system biomass). After each hourly timestep, soil water budget was updated based on net flux for each layer from root exchange, soil evaporation, and vertical fluxes between layers including infiltration of precipitation. All incident precipitation infiltrated instantly to field capacity from the top down, with any excess draining from the bottom of the root zone. Outside of the GS transpiration and soil evaporation were assumed zero. Off-season activity of evergreen conifers was not modeled. With no interception or runoff and no water loss in the off season besides vertical drainage, the simulations represent maximum possible usage of GS precipitation and maximum recharge from off-season precipitation.

Stand LAI was adjusted by altering BAI to satisfy ecohydrologic equilibrium for historic conditions (Fig. 2). To ascertain equilibrium, 35 y were simulated starting from a soil profile at field capacity. After a 5-y burn-in period to allow the soil moisture profile to adjust, the annual PLC_{max} was averaged over the remaining 30 y. The greater the BAI and LAI, the faster the stand consumed water, and the greater the 30-y mean PLC_{max}. A mean PLC_{max} of 10 represented the chronic stress threshold (Fig. 2). Mortality was indicated if PLC_{max} in any single year exceeded 85 (Fig. 2, upper mortality line) based on the results of Venturas et al. (36). Ecohydrologic equilibrium was attained when LAI was maximized without pushing the stand across either threshold. Stand acclimation to future conditions followed the same process.

The mean equilibrium BAI is influenced by rooting depth (Rd), an important parameter with considerable uncertainty. To better constrain Rd, we first used one of the deeper depths in the literature (Dataset S3). If the resulting mean equilibrium BAI was equal or lower than the reported mean BAI of Forest Inventory of America (FIA) plots where the species was dominant (Dataset S3) we kept that Rd for the species. If the equilibrium BAI was greater than the FIA mean, the Rd was reduced to make the equilibrium BAI mean 5% or less below the FIA mean. As for other species-specific (non-plastic) inputs, the Rd was equal across species sites and between historic and future simulations.

Biomass and Respiration. Leaf biomass (kilograms per hectare) was calculated for all scenarios dividing the allometric LAI (square meters per hectare) by specific LA (square meters per kilogram; Dataset S3). We used species-specific allometric equations for calculating total above-ground biomass (AGB, kilograms per hectare) and stem biomass (kilograms per hectare) based on

DBH and leaf biomass (Dataset S3). We used the same relationship for estimating root biomass from AGB for all species (106).

Leaf respiration during the GS is accounted for in the gain–risk algorithm which calculates net canopy assimilation on an annual basis per ground area (A_{net}, kilograms of carbon per hectare per year). Conifer leaf respiration in winter was neglected (107), and modeled angiosperms were deciduous; therefore, we did not calculate A_{net} out of the GS. Annual woody (stem and root) respiration ($Resp_{wood}$; kilograms of carbon per hectare per year) was summed over hourly increments (103):

$$Resp_{wood} = \sum \left(Biomass \cdot \left(\frac{r_{15}}{8,760} \right) \cdot q_{10}^{\frac{T-15}{10}} \right),$$

where Biomass is the stem plus root biomass (kilograms of carbon), q_{10} a dimensionless temperature coefficient, r_{15} the maintenance respiration parameter (kilograms of carbon per kilogram of sapwood carbon per year), and T the air temperature (degrees Celsius) of each hour. We used $q_{10} = 1.4$ and $r_{15} = 0.01$ for angiosperms and $q_{10} = 1.7$ and $r_{15} = 0.025$ for gymnosperms (103). We used a 0.5 conversion factor for transforming biomass from kilograms per hectare to kilograms of carbon per hectare (108). NPP per ground area was calculated on an annual basis as NPP = $A_{net} − Resp_{wood}$.

Data Analysis. The model output for NPP, stand E, mean PLC_{max}, and assimilation-weighted C_i/C_a were mean annual values over the 30 simulation years. Percent changes are with respect to historic weather and C_a. Temperature increases (ΔT) were future minus historic average GS temperature. Mortality percentage was based on the number of location+species+ESM simulations (for a given C_a) that exceeded $PLC_{max} = 85$ in any of the 30 simulation years. "Future" simulations ($\Delta C_a\Delta T$) were for RCP-defined ΔC_a and the corresponding ESM defined weather and ΔT. "Enrichment" simulations (ΔC_a) were for RCP-defined ΔC_a and historic weather ($\Delta T = 0$). "Warming-only" simulations (ΔT) were for the same ESM-defined weather and ΔT used for future simulations, but with historic C_a ($\Delta C_a = 0$). For generating the contours in Fig. 7, 2 additional simulations were run that 1) combined RCP4.5 ΔC_a with RCP8.5 weather (ΔT) and 2) RCP8.5 ΔC_a with RCP4.5 weather (ΔT). Contours in Fig. 7 were based on linear regressions between all ΔT's (for both RCP4.5 and 8.5 weathers) and mean PLC_{max} (Fig. 7*A*), NPP (Fig. 7*B*), and AGB (Fig. 7*C*) at each of 3 ΔC_a: 0, 177 ppm (RCP4.5), and 449 ppm (RCP 8.5). ANOVAs were used to partition variation in model output between site, ESM, and species [Y ∼ ESM(site) + species(site)].

Data and Code Availability. The gain–risk model code (written in C++), the acclimation codes (Visual Basic Macros), the simulated hourly weather data used for running simulations, and the main model output data are publicly available at Figshare (DOI: 10.6084/m9.figshare.8805110) (109).

1. IPCC, Global warming of 1.5 °C: An IPCC special report on the impacts of global warming of 1.5°C above pre-industrial levels and related global greenhouse gas emission pathways, in the context of strengthening the global response to the threat of climate change, sustainable development, and efforts to eradicate poverty, V. Masson-Delmotte *et al.*, Eds. (Intergovernmental Panel on Climate Change, Geneva, Switzerland, 2018).
2. M. E. Dusenge, A. G. Duarte, D. A. Way, Plant carbon metabolism and climate change: Elevated CO₂ and temperature impacts on photosynthesis, photorespiration and respiration. *New Phytol.* **221**, 32–49 (2019).
3. E. A. Ainsworth, S. P. Long, What have we learned from 15 years of free-air CO2 enrichment (FACE)? A meta-analytic review of the responses of photosynthesis, canopy properties and plant production to rising CO2. *New Phytol.* **165**, 351–371 (2005).
4. R. J. Norby, D. R. Zak, Ecological lessons from free-air CO2 enrichment (FACE) experiments. *Annu. Rev. Ecol. Evol. Syst.* **42**, 181–203 (2011).
5. T. F. Keenan *et al.*, Recent pause in the growth rate of atmospheric CO₂ due to enhanced terrestrial carbon uptake. *Nat. Commun.* **7**, 13428 (2016).

6. K. A. Novick, C. F. Miniat, J. M. Vose, Drought limitations to leaf-level gas exchange: Results from a model linking stomatal optimization and cohesion-tension theory. *Plant Cell Environ.* **39**, 583–596 (2016).
7. K. Mott, D. Parkhurst, Stomatal responses to humidity in air and helox. *Plant Cell Environ.* **14**, 509–515 (1991).
8. R. E. Will, S. M. Wilson, C. B. Zou, T. C. Hennessey, Increased vapor pressure deficit due to higher temperature leads to greater transpiration and faster mortality during drought for tree seedlings common to the forest-grassland ecotone. *New Phytol.* **200**, 366–374 (2013).
9. C. Allen *et al.*, A global overview of drought and heat-induced tree mortality reveals emerging climate change risks for forests. *For. Ecol. Manage.* **259**, 660–684 (2010).
10. C. D. Allen, D. D. Breshears, N. G. McDowell, On underestimation of global vulnerability to tree mortality and forest die-off from hotter drought in the Anthropocene. *Ecosphere* **6**, 1–55 (2015).
11. F. Babst *et al.*, Twentieth century redistribution in climatic drivers of global tree growth. *Sci. Adv.* **5**, eaat4313 (2019).

12. K. C. Guay *et al.*, Vegetation productivity patterns at high northern latitudes: A multi-sensor satellite data assessment. *Glob. Change Biol.* **20**, 3147–3158 (2014).

13. Z. e. Gedalof, A. A. Berg, Tree ring evidence for limited direct CO2 fertilization of forests over the 20th century. *Global Biogeochem. Cycles* **24**, GB3027 (2010).

14. C. Körner, Plant CO2 responses: An issue of definition, time and resource supply. *New Phytol.* **172**, 393–411 (2006).

15. Y. Wang *et al.*, The stomatal response to rising CO$_2$ concentration and drought is predicted by a hydraulic trait-based optimization model. *Tree Physiol.* **39**, 1416–1427 (2019).

16. L. Benomar *et al.*, Genetic adaptation vs. ecophysiological plasticity of photosynthetic-related traits in young *Picea glauca* trees along a regional climatic gradient. *Front. Plant Sci.* **7**, 48 (2016).

17. J. L. Carter, D. A. White, Plasticity in the Huber value contributes to homeostasis in leaf water relations of a mallee Eucalypt with variation to groundwater depth. *Tree Physiol.* **29**, 1407–1418 (2009).

18. S. Dillon, A. Quentin, M. Ivković, R. T. Furbank, E. Pinkard, Photosynthetic variation and responsiveness to CO2 in a widespread riparian tree. *PLoS One* **13**, e0189635 (2018).

19. D. A. Way, R. Oren, Differential responses to changes in growth temperature between trees from different functional groups and biomes: A review and synthesis of data. *Tree Physiol.* **30**, 669–688 (2010).

20. R. A. Fisher *et al.*, Vegetation demographics in Earth System Models: A review of progress and priorities. *Glob. Change Biol.* **24**, 35–54 (2018).

21. G. B. Bonan, M. Williams, R. A. Fisher, K. W. Oleson, Modeling stomatal conductance in the earth system: Linking leaf water-use efficiency and water transport along the soil-plant-atmosphere continuum. *Geosci. Model Dev.* **7**, 2193–2222 (2014).

22. J. T. Ball, I. E. Woodrow, J. A. Berry, "A model predicting stomatal conductance and its contribution to the control of photosynthesis under different environmental conditions" in *Progress in Photosynthesis Research*, J. Biggins, Ed. (Martinus Nijhoff, The Netherlands, 1987), **vol. 4**, pp. 221–224.

23. R. Leuning, A critical appraisal of a coupled stomatal-photosynthesis model for C3 plants. *Plant Cell Environ.* **18**, 339–357 (1995).

24. T. L. Powell *et al.*, Confronting model predictions of carbon fluxes with measurements of Amazon forests subjected to experimental drought. *New Phytol.* **200**, 350–365 (2013).

25. R. Oren, N. Phillips, B. E. Ewers, D. E. Pataki, J. P. Megonigal, Sap-flux-scaled transpiration responses to light, vapor pressure deficit, and leaf area reduction in a flooded Taxodium distichum forest. *Tree Physiol.* **19**, 337–347 (1999).

26. L. A. Cernusak *et al.*, Environmental and physiological determinants of carbon isotope discrimination in terrestrial plants. *New Phytol.* **200**, 950–965 (2013).

27. A. T. Trugman *et al.*, Climate and plant trait strategies determine tree carbon allocation to leaves and mediate future forest productivity. *Glob. Change Biol.* **25**, 3395–3405 (2019).

28. A. T. Trugman *et al.*, Leveraging plant hydraulics to yield predictive and dynamic plant leaf allocation in vegetation models with climate change. *Glob. Change Biol.*, 10.1111/gcb.14814 (2019).

29. T. J. Brodribb, Xylem hydraulic physiology: The functional backbone of terrestrial plant productivity. *Plant Sci.* **177**, 245–251 (2009).

30. J. S. Sperry, Hydraulic constraints on plant gas exchange. *Agric. For. Meteorol.* **104**, 13–23 (2000).

31. H. D. Adams *et al.*, A multi-species synthesis of physiological mechanisms in drought-induced tree mortality. *Nat. Ecol. Evol.* **1**, 1285–1291 (2017).

32. W. R. L. Anderegg *et al.*, Tree mortality predicted from drought-induced vascular damage. *Nat. Geosci.* **8**, 367–371 (2015).

33. L. Rowland *et al.*, Death from drought in tropical forests is triggered by hydraulics not carbon starvation. *Nature* **528**, 119–122 (2015).

34. M. D. Venturas *et al.*, Chaparral shrub hydraulic traits, size, and life history types relate to species mortality during California's historic drought of 2014. *PLoS One* **11**, e0159145 (2016).

35. B. Choat *et al.*, Triggers of tree mortality under drought. *Nature* **558**, 531–539 (2018).

36. M. D. Venturas *et al.*, A stomatal control model based on optimization of carbon gain versus hydraulic risk predicts aspen sapling responses to drought. *New Phytol.* **220**, 836–850 (2018).

37. W. M. Hammond *et al.*, Dead or dying? Quantifying the point of no return from hydraulic failure in drought-induced tree mortality. *New Phytol.* **223**, 1834–1843 (2019).

38. C. B. Field, N. M. Holbrook, Catastrophic xylem failure: Life at the brink. *Trends Ecol. Evol.* **4**, 124–126 (1989).

39. J. P. Sparks, R. A. Black, Regulation of water loss in populations of *Populus trichocarpa*: The role of stomatal control in preventing xylem cavitation. *Tree Physiol.* **19**, 453–459 (1999).

40. J. S. Sperry *et al.*, Predicting stomatal responses to the environment from the optimization of photosynthetic gain and hydraulic cost. *Plant Cell Environ.* **40**, 816–830 (2017).

41. A. Wolf, W. R. L. Anderegg, S. W. Pacala, Optimal stomatal behavior with competition for water and risk of hydraulic impairment. *Proc. Natl. Acad. Sci. U.S.A.* **113**, E7222–E7230 (2016).

42. W. R. L. Anderegg *et al.*, Woody plants optimise stomatal behaviour relative to hydraulic risk. *Ecol. Lett.* **21**, 968–977 (2018).

43. S. L. Voelker *et al.*, A dynamic leaf gas-exchange strategy is conserved in woody plants under changing ambient CO2 : Evidence from carbon isotope discrimination in paleo and CO2 enrichment studies. *Glob. Change Biol.* **22**, 889–902 (2016).

44. T. N. Buckley, The role of stomatal acclimation in modelling tree adaptation to high CO2. *J. Exp. Bot.* **59**, 1951–1961 (2008).

45. J. R. Ehleringer, T. E. Cerling, Atmospheric CO(2) and the ratio of intercellular to ambient CO(2) concentrations in plants. *Tree Physiol.* **15**, 105–111 (1995).

46. N. G. Smith *et al.*, Global photosynthetic capacity is optimized to the environment. *Ecol. Lett.* **22**, 506–517 (2019).

47. V. Maire *et al.*, Global effects of soil and climate on leaf photosynthetic traits and rates. *Glob. Ecol. Biogeogr.* **24**, 706–717 (2015).

48. M. Westoby, D. Warton, P. B. Reich, The time value of leaf area. *Am. Nat.* **155**, 649–656 (2000).

49. H. Poorter *et al.*, Construction costs, chemical composition and payback time of high- and low-irradiance leaves. *J. Exp. Bot.* **57**, 355–371 (2006).

50. O. Franklin *et al.*, Modeling carbon allocation in trees: A search for principles. *Tree Physiol.* **32**, 648–666 (2012).

51. P. S. Eagleson, Ecological optimality in water-limited natural soil-vegetation systems: 1. Theory and hypothesis. *Water Resour. Res.* **18**, 325–340 (1982).

52. D. M. Love *et al.*, Dependence of aspen stands on a subsurface water subsidy: Implications for climate change impacts. *Water Resour. Res.* **55**, 1833–1848 (2019).

53. A. Cabon, J. Martínez-Vilalta, J. Martínez de Aragón, R. Poyatos, M. De Cáceres, Applying the eco-hydrological equilibrium hypothesis to model root distribution in water-limited forests. *Ecohydrology* **11**, e2015 (2018).

54. J. Yang, B. E. Medlyn, M. G. De Kauwe, R. A. Duursma, Applying the concept of ecohydrological equilibrium to predict steady state leaf area index. *J. Adv. Model. Earth Syst.* **10**, 1740–1758 (2018).

55. N. G. McDowell, C. D. Allen, Darcy's law predicts widespread forest mortality under climate warming. *Nat. Clim. Chang.* **5**, 669–672 (2015).

56. A. P. Williams *et al.*, Temperature as a potent driver of regional forest drought stress and tree mortality. *Nat. Clim. Chang.* **3**, 292–297 (2013).

57. D. J. Young *et al.*, Long-term climate and competition explain forest mortality patterns under extreme drought. *Ecol. Lett.* **20**, 78–86 (2017).

58. L. D'Orangeville *et al.*, Drought timing and local climate determine the sensitivity of eastern temperate forests to drought. *Glob. Change Biol.* **24**, 2339–2351 (2018).

59. N. Pederson *et al.*, The legacy of episodic climatic events in shaping temperate, broadleaf forests. *Ecol. Monogr.* **84**, 599–620 (2014).

60. E. G. Bobich, G. A. Barron-Gafford, K. G. Rascher, R. Murthy, Effects of drought and changes in vapour pressure deficit on water relations of Populus deltoides growing in ambient and elevated CO2. *Tree Physiol.* **30**, 866–875 (2010).

61. P. B. Reich *et al.*, Effects of climate warming on photosynthesis in boreal tree species depend on soil moisture. *Nature* **562**, 263–267 (2018).

62. M. R. Carins Murphy, G. J. Jordan, T. J. Brodribb, Acclimation to humidity modifies the link between leaf size and the density of veins and stomata. *Plant Cell Environ.* **37**, 124–131 (2014).

63. M. J. Hovenden, J. K. Vander Schoor, Y. Osanai, Relative humidity has dramatic impacts on leaf morphology but little effect on stomatal index or density in Nothofagus cunninghamii (Nothofagaceae). *Aust. J. Bot.* **60**, 700–706 (2012).

64. M. Mencuccini, J. Grace, Climate influences the leaf area/sapwood area ratio in Scots pine. *Tree Physiol.* **15**, 1–10 (1995).

65. D. White, C. Beadle, D. Worledge, J. Honeysett, M. Cherry, The influence of drought on the relationship between leaf and conducting sapwood area in Eucalyptus globulus and Eucalyptus nitens. *Trees* **12**, 406–414 (1998).

66. R. M. Callaway, E. H. DeLucia, W. H. Schlesinger, Biomass allocation of montane and desert ponderosa pine: An analog for response to climate change. *Ecology* **75**, 1474–1481 (1994).

67. T. Rosas *et al.*, Adjustments and coordination of hydraulic, leaf and stem traits along a water availability gradient. *New Phytol.* **223**, 632–646 (2019).

68. N. A. McBranch *et al.*, Lack of acclimation of leaf area:sapwood area ratios in piñon pine and juniper in response to precipitation reduction and warming. *Tree Physiol.* **39**, 135–142 (2019).

69. M. P. Thakur *et al.*, Soil microbial, nematode, and enzymatic responses to elevated CO2, N fertilization, warming, and reduced precipitation. *Soil Biol. Biochem.* **135**, 184–193 (2019).

70. P. E. Thornton, J. F. Lamarque, N. A. Rosenbloom, N. M. Mahowald, Influence of carbon-nitrogen cycle coupling on land model response to CO2 fertilization and climate variability. *Global Biogeochem. Cycles* **21**, GB4018 (2007).

71. R. J. Norby, J. M. Warren, C. M. Iversen, B. E. Medlyn, R. E. McMurtrie, CO2 enhancement of forest productivity constrained by limited nitrogen availability. *Proc. Natl. Acad. Sci. U.S.A.* **107**, 19368–19373 (2010).

72. R. Oren *et al.*, Soil fertility limits carbon sequestration by forest ecosystems in a CO2-enriched atmosphere. *Nature* **411**, 469–472 (2001).

73. R. S. Nowak, D. S. Ellsworth, S. D. Smith, Functional responses of plants to elevated atmospheric CO2–do photosynthetic and productivity data from FACE experiments support early predictions? *New Phytol.* **162**, 253–280 (2004).

74. J. C. Domec, D. D. Smith, K. A. McCulloh, A synthesis of the effects of atmospheric carbon dioxide enrichment on plant hydraulics: Implications for whole-plant water use efficiency and resistance to drought. *Plant Cell Environ.* **40**, 921–937 (2017).

75. A. L. Jacobsen, R. B. Pratt, S. D. Davis, M. F. Tobin, Geographic and seasonal variation in chaparral vulnerability to cavitation. *Madrono* **61**, 317–327 (2014).

76. Y. Liu *et al.*, Increasing atmospheric humidity and CO2 concentration alleviate forest mortality risk. *Proc. Natl. Acad. Sci. U.S.A.* **114**, 9918–9923 (2017).

77. C. Huntingford *et al.*, Simulated resilience of tropical rainforests to CO 2-induced climate change. *Nat. Geosci.* **6**, 268 (2013).

78. H. Hartmann *et al.*, Research frontiers for improving our understanding of drought-induced tree and forest mortality. *New Phytol.* **218**, 15–28 (2018).

79. M. Chahine *et al.*, Satellite remote sounding of mid-tropospheric CO$_2$. *Geophys. Res. Lett.* **35**, L17807 (2008).

80. P. Ciais *et al.*, "Carbon and other biogeochemical cycles" in *Climate Change 2013: The Physical Science Basis. Contribution of Working Group I to the Fifth Assessment Report of the Intergovernmental Panel on Climate Change* (Cambridge University Press, 2014), pp. 465–570.

81. N. D. Charney et al., Observed forest sensitivity to climate implies large changes in 21st century North American forest growth. *Ecol. Lett.* **19**, 1119–1128 (2016).

82. D. Schimel, B. B. Stephens, J. B. Fisher, Effect of increasing CO2 on the terrestrial carbon cycle. *Proc. Natl. Acad. Sci. U.S.A.* **112**, 436–441 (2015).

83. P. M. Cox, R. A. Betts, C. D. Jones, S. A. Spall, I. J. Totterdell, Acceleration of global warming due to carbon-cycle feedbacks in a coupled climate model. *Nature* **408**, 184–187 (2000).

84. Y. Malhi et al., Exploring the likelihood and mechanism of a climate-change-induced dieback of the Amazon rainforest. *Proc. Natl. Acad. Sci. U.S.A.* **106**, 20610–20615 (2009).

85. J. E. Duffy, C. M. Godwin, B. J. Cardinale, Biodiversity effects in the wild are common and as strong as key drivers of productivity. *Nature* **549**, 261–264 (2017).

86. M. Mencuccini, S. Manzoni, B. Christoffersen, Modelling water fluxes in plants: From tissues to biosphere. *New Phytol.* **222**, 1207–1222 (2019).

87. R. M. Burns, B. H. Honkala, *Silvics of North America: Volume 1. Conifers. Volume 2. Hardwoods* (US Department of Agriculture Forest Service, 1990), p. 654.

88. J. Horel et al., Mesowest: Cooperative mesonets in the western United States. *Bull. Am. Meteorol. Soc.* **83**, 211–225 (2002).

89. Soil Survey Staff, Natural Resources Conservation Service, United States Department of Agriculture, Web Soil Survey. https://websoilsurvey.nrcs.usda.gov. Accessed 10 October 2018.

90. K. E. Taylor, R. J. Stouffer, G. A. Meehl, An overview of CMIP5 and the experiment design. *Bull. Am. Meteorol. Soc.* **93**, 485–498 (2012).

91. M. Wise et al., Implications of limiting CO2 concentrations for land use and energy. *Science* **324**, 1183–1186 (2009).

92. S. J. Smith, T. M. L. Wigley, Multi-gas forcing stabilization with minicam. *Energy J.* **27**, 373–391 (2006).

93. K. Riahi, A. Grübler, N. Nakicenovic, Scenarios of long-term socio-economic and environmental development under climate stabilization. *Technol. Forecast. Soc. Change* **74**, 887–935 (2007).

94. S. Fatichi, V. Y. Ivanov, E. Caporali, Simulation of future climate scenarios with a weather generator. *Adv. Water Resour.* **34**, 448–467 (2011).

95. V. Y. Ivanov, R. L. Bras, D. C. Curtis, A weather generator for hydrological, ecological, and agricultural applications. *Water Resour. Res.* **43**, W10406 (2007).

96. M. Marani, On the correlation structure of continuous and discrete point rainfall. *Water Resour. Res.* **39**, 1128 (2003).

97. Y. H. Fu, M. Campioli, G. Deckmyn, I. A. Janssens, The impact of winter and spring temperatures on temperate tree budburst dates: Results from an experimental climate manipulation. *PLoS One* **7**, e47324 (2012).

98. K. J. Niklas, The allometry of safety-factors for plant height. *Am. J. Bot.* **81**, 345–351 (1994).

99. B. T. Wolfe, J. S. Sperry, T. A. Kursar, Does leaf shedding protect stems from cavitation during seasonal droughts? A test of the hydraulic fuse hypothesis. *New Phytol.* **212**, 1007–1018 (2016).

100. B. E. Medlyn et al., Temperature response of parameters of a biochemically based model of photosynthesis. II. A review of experimental data. *Plant Cell Environ.* **25**, 1167–1179 (2002).

101. C. Bernacchi, E. Singsaas, C. Pimentel, A. Portis, Jr, S. Long, Improved temperature response functions for models of Rubisco-limited photosynthesis. *Plant Cell Environ.* **24**, 253–259 (2001).

102. R. Leuning, Temperature dependence of two parameters in a photosynthesis model. *Plant Cell Environ.* **25**, 1205–1210 (2002).

103. M. B. Lavigne, M. G. Ryan, Growth and maintenance respiration rates of aspen, black spruce and jack pine stems at northern and southern BOREAS sites. *Tree Physiol.* **17**, 543–551 (1997).

104. N. J. Bréda, Ground-based measurements of leaf area index: A review of methods, instruments and current controversies. *J. Exp. Bot.* **54**, 2403–2417 (2003).

105. G. S. Campbell, J. N. Norman, *An Introduction to Environmental Biophysics* (Springer, New York, ed. 2, 1998).

106. M. A. Cairns, S. Brown, E. H. Helmer, G. A. Baumgardner, Root biomass allocation in the world's upland forests. *Oecologia* **111**, 1–11 (1997).

107. G. Wieser, Carbon dioxide gas exchange of cembran pine (Pinus cembra) at the alpine timberline during winter. *Tree Physiol.* **17**, 473–477 (1997).

108. E. V. Carey, E. H. DeLucia, J. T. Ball, Stem maintenance and construction respiration in Pinus ponderosa grown in different concentrations of atmospheric CO(2). *Tree Physiol.* **16**, 125–130 (1996).

109. J. S. Sperry et al., Dataset and Code: The impact of rising CO2 and acclimation on the response of US forests to global warming. Figshare. https://figshare.com/articles/Dataset_and_Code_The_impact_of_rising_CO2_and_acclimation_on_the_response_of_US_forests_to_global_warming/8805110. Deposited 5 November 2019.